Synthesis, characterization and thermal behaviour of $Fe_{0.65}Co_{0.35}$-$MgAl_2O_4$ and $Fe_{0.65}Ni_{0.35}$-$MgAl_2O_4$ nanocomposite powders

Olivier Quénard,[a] Eddy De Grave,[b] Christophe Laurent*[a†] and Abel Rousset[a]

[a]*Laboratoire de Chimie des Matériaux Inorganiques, ESA CNRS 5070, Université Paul-Sabatier, 31062 Toulouse cedex 4, France*

[b]*NUMAT, Department of Subatomic and Radiation Physics, University of Gent, Proeftuinstraat 86, B-9000 Gent, Belgium*

$Fe_{0.65}Co_{0.35}$-$MgAl_2O_4$ and $Fe_{0.65}Ni_{0.35}$-$MgAl_2O_4$ nanocomposite powders are prepared by selective hydrogen reduction of monophasic oxide solid solutions synthesized by combustion in urea. The alloy particles, which are dispersed in the spinel matrix, are about 10 nm in size. An increase in reduction temperature from 700 to 1000 °C produces a narrowing of the particles' composition range and an average composition closer to the target one. The magnetic nature of the alloy nanoparticles is discussed. The nanoparticles dispersed inside the oxide grains, which account for more than two thirds of the total metallic phase, are stable in air up to *ca.* 800 °C.

The enhanced or novel properties of ceramic-matrix nanocomposites have triggered worldwide research efforts in recent years, notably prompting the emergence of challenging synthesis routes.[1–4] The dispersion of nanometric particles inside ceramic grains is of particular interest since one obtains not only a potentially interesting composite material, but also an easy to handle, stable nanodispersoid that may be used for basic research related to the division state of solids. This laboratory has proposed a novel method based on the selective hydrogen reduction of homogeneous solid solutions between two or more metallic oxides for the synthesis of metal–oxide nanocomposite powders such as Fe/Cr-Al_2O_3,[5,6] Fe/Ni- and Fe/Ru-Al_2O_3,[7] Fe/Cr-Cr_2O_3,[8] Fe- and Fe/Ni-MgO.[9,10] In these materials, transition-metal or alloy particles are generally smaller than 10 nm and are dispersed within the grains of the oxide matrix. However, several factors including the metal content, the mutual solubility of the parent oxides, the specific surface area and the crystalline state of the starting oxide solid solution can modify the size, size distribution and location (inside or at the surface of the oxide grains) of the metal particles. Furthermore, the intragranular metal particles can either be directly epitaxied with the oxide lattice or separated from it by an interfacial phase a few nanometers thick.[11,12] More recently, Co- and Ni-$MgAl_2O_4$ powders have been prepared by this method.[13] The present work deals with the synthesis and characterization of Fe/Co-and Fe/Ni-$MgAl_2O_4$ powders. The aim was to prepare $MgAl_2O_4$-based oxide phases containing homogeneously dispersed transition-metal ions substituting for Mg^{2+} and to investigate the reduction behaviour of these oxides with respect to the formation of the composite powder and to determine the composition of the metal particles. A total reduction of the transition metal ions would yield $Fe_{0.65}Co_{0.35}$- and $Fe_{0.65}Ni_{0.35}$-$MgAl_2O_4$ composites. This particular composition was chosen because it is in the range of the so-called Invar Fe/Ni alloys, which present unusual properties such as a small thermal expansion coefficient, a sudden decrease of the spontaneous magnetization and a high magnetic susceptibility.[14–16] It may be of interest to investigate such alloys in the form of nanometric particles embedded in a $MgAl_2O_4$ matrix rather than as unsupported particles or in bulk form, which have been extensively studied before.

† E-mail: laurent@iris.ups-tlse.fr

Experimental

The appropriate amounts of the desired metal nitrates (Mg, Al, Fe, Co, Ni) were mixed in stoichiometric proportions with urea and dissolved in the minimum amount of water in a Pyrex vessel. It should be noted that the transition-metal nitrates were added in substitution for Mg nitrate. The stoichiometric composition of the redox mixtures was calculated using the total oxidizing and reducing valency of the metal nitrates (oxidizer) and urea (fuel), which serve as numerical coefficients for the stoichiometric balance, so that the equivalence ratio is equal to unity.[17–19] The vessel containing the solution was inserted into a furnace pre-heated at 600 °C. The solution immediately started to boil and undergo dehydration. The decomposition of the metal nitrates was accompanied by a large release of gases (oxides of nitrogen and ammonia). The obtained paste frothed and formed a foam which swelled and then blazed up. A white flame occurred with the production of a material which swelled to the capacity of the Pyrex vessel. The total combustion process takes place in less than 5 min. One combustion batch yields about 6 g of powder. The combustion products were mechanically ground using zirconia balls and vessel, giving rise to the hereafter designated 'as-prepared' oxide powders. The as-prepared oxides were reduced for 1 h in dry hydrogen at different temperatures (T_r) as required for the study. A total reduction of the transition metal ions would yield 4 mass% of metallic phase in the thus-obtained metal–oxide composite powders.

Elemental analysis was performed by atomic absorption spectroscopy. Phase detection and identification was carried out by X-ray diffraction (XRD) analysis [λ(Co-Kα)= 0.17902 nm]. The lattice parameters were calculated from the XRD patterns using NaCl as internal standard. Specific-surface-area (S_w) measurements were performed using nitrogen and krypton adsorption for the oxide and composite powders respectively. The powders were also studied by scanning electron microscopy (SEM), transmission electron microscopy (TEM) and electron microdiffraction (EMD) analysis. The composition of the metal nanoparticles was evaluated by TEM energy-dispersive X-ray spectroscopy (EDX) from the results of about 20 analyses per composite powder (spot diameter equal to 2 or 7 nm according to the size of the particle under investigation). SEM specimens were prepared by ultrasonic dispersion in ethanol, deposited onto an aluminium sample holder and coated with Ag to prevent charge accumulation.

The powders for TEM examination were sonicated in ethanol and a drop of the dispersion was deposited onto a copper grid coated with a collodion film. The oxidation of the composite powders was investigated by thermogravimetry (TG) in flowing air (heating rate 3 °C min^{-1}).

^{57}Fe Mössbauer spectra were recorded with a ^{57}Co (Rh) source in a conventional time-mode spectrometer with constant-acceleration drive and a triangular reference signal. The spectra for the oxides and nanocomposite powders, were collected with the absorbers at 9 K and also at 298 K for some specimens. One spectrum was run at 275 K in an external field of 6 T applied parallel to the γ-ray beam. Accumulation of the data was performed in 1024 channels until a background of at least 10^6 counts per channel was reached. The spectrometer was calibrated by collecting at room temperature the spectrum of a standard Fe foil and the centre shift (δ) values quoted hereafter are with reference to this standard (centre shift = intrinsic isomer shift + second order Doppler shift). The Mössbauer spectra of the Fe/Co-$MgAl_2O_4$ samples were analysed assuming symmetrical components with a Lorentzian line shape, while those of the oxides and those of the Fe/Ni-$MgAl_2O_4$ composites were fitted with a hyperfine field distribution (each subspectrum of the distribution is composed of Lorentzian lines). This latter procedure was chosen because the corresponding Mössbauer patterns were strongly asymmetrical.

Results and Discussion

Oxides

Elemental analysis (Table 1) shows that the as-prepared oxides contain the desired proportions of Mg, Al, Fe and Co or Ni. As expected, the Co-containing powder is dark blue and the Ni-containing powder is green–grey. The only phase detected on both XRD patterns is the desired spinel (Fig. 1). The lattice parameter measured for both oxides ($a = 0.8085$ nm) is in good agreement with that calculated using Vegard's law (0.8086 nm and 0.8084 nm for $Mg_{0.9}Fe_{0.065}Co_{0.035}Al_2O_4$ and $Mg_{0.9}Fe_{0.065}Ni_{0.035}Al_2O_4$ respectively). These results show that the presence of iron promotes the formation of monophase products: indeed, it has been shown in a previous work[13] that similar Fe-free compounds ($Mg_{0.9}M_{0.1}Al_2O_4$, M = Co, Ni) consist in fact of a mixture of MgO (in very small amount) and a spinel phase, which thus contains an excess of trivalent cations. This finding is consistent with the MgO–Al_2O_3 phase diagram[20] which indeed indicates that the spinel phase may be non-stoichiometric at temperatures similar to the one reached in the combustion process (*ca.* 1200 °C). Moreover, Navrotsky and Kleppa[21] pointed out that a considerable solid-solution range exists on the Al_2O_3-rich side of the stoichiometric NAl_2O_4 (N = Mg, Mn, Fe, Co, Ni, Cu) spinels.

Table 1 Elemental analysis (±2 mass%) and some characteristics of the as-prepared oxides; a = lattice parameter/nm; S_w = specific surface area/$m^2\ g^{-1}$

Mg	Al	Fe	Co	Ni	phase (XRD)	a	color	S_w
14.7	36.5	2.5	1.4	—	spinel	0.8085	dark blue	5.6
14.8	36.5	2.6	—	1.4	spinel	0.8085	grey	6.0

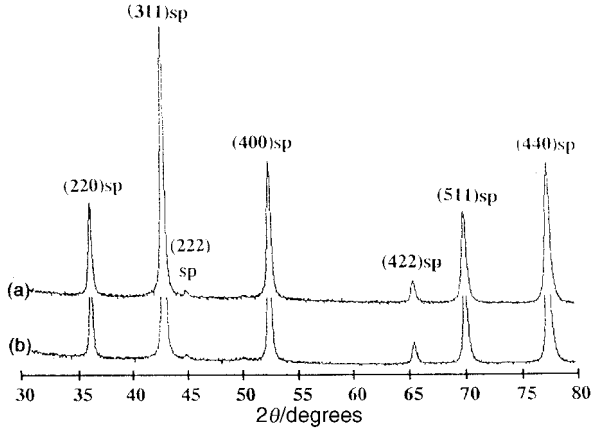

Fig. 1 XRD patterns of the as-prepared (a) Co- and (b) Ni-containing oxides (sp, spinel phase)

Mössbauer spectra of the as-prepared oxides at 9 K are shown in Fig. 2. At this temperature, the electron hopping that may occur between iron(II) and iron(III) ions located in the octahedral sites is suppressed. The best fit was obtained assuming a superposition of two quadrupole-splitting distributions (accounting for the Fe^{2+} and Fe^{3+} ions), their values being linearly correlated with the centre shifts. The corresponding Mössbauer parameters are given in Table 2. The quadrupole splitting distribution profiles of the two components both show two peaks, that one is tempted to relate to tetrahedral and octahedral sites. However, the data obtained so far do not allow one to make such a specific assignment. It is interesting, though, that the values of the Fe^{3+} quadrupole-splitting peaks are markedly lower for the Co–oxide (0.40 and 0.95 mm s^{-1}) than for the Ni–oxide (0.75 and 1.55 mm s^{-1}). The presence of Fe^{3+} ions implies that the as-prepared powders are not solid solutions between $MgAl_2O_4$, $FeAl_2O_4$ and MAl_2O_4 (M = Co, Ni) only, as expected, but that at least a fourth component (such as γ-Fe_2O_3, Fe_3O_4 or $MgFe_2O_4$) is involved in the solid solution. It is noteworthy that Fe^{3+} ions predominate over Fe^{2+} ions (Table 2). This observed excess of trivalent ions leads for the involved spinels to a $D_{1-\alpha}T_{2+2\alpha/3}O_4$ general formula, where D and T stand for divalent and trivalent cations respectively. Navrotsky and Kleppa[21] proposed that spinel structures on the Al_2O_3-rich side of the stoichiometric NAl_2O_4 compound can be described as solid solutions between the stoichiometric NAl_2O_4 and the metastable defective spinel structure γ-Al_2O_3, the vacancies being distributed either on the tetrahedral or on the octahedral sites, or on both. Thus, one possibility would be to describe the present oxides as a solid solution between stoichiometric (Mg, Fe, M)Al_2O_4 and γ-(Fe, Al)$_2O_3$, with M = Co, Ni. It is likely that the Fe^{3+} ions are located at or near the surface of the oxide crystallites since they become fully reduced [to the iron(II) state] at a temperature as low as 700 °C as shown by the Mössbauer spectra presented later in this paper. This finding suggests the presence of concentration gradients within a given crystallite, the proportion of Fe^{2+} ions decreasing, and that of Fe^{3+} ions and vacancies increasing, from the core to the surface. More work is in progress to gain a better understanding of the nature of the $M'M''_2O_4$ ($M' = Mg^{2+}$, Fe^{2+}, Co^{2+}, Ni^{2+}; $M'' = Al^{3+}$, Fe^{3+}) oxides.

The specific surface area of the as-prepared powders is close to 6 $m^2\ g^{-1}$ (Table 1), which is lower than those of $Mg_{0.9}Co_{0.1}Al_2O_4$ and $Mg_{0.9}Ni_{0.1}Al_2O_4$ solid solutions obtained by the same route ($10 \leqslant S_w \leqslant 20$ $m^2\ g^{-1}$)[13] and also lower than that measured by Kingsley and Patil[17] for $MgAl_2O_4$ (21.8 $m^2\ g^{-1}$). This difference could arise owing to the use of a higher mass/volume ratio in the combustion experiments of the present study. SEM observations (Fig. 3) of the oxides show that the powders consist of platelet-like grains, the surfaces of which present some porosity resulting from the escaping of gases during the combustion process. TEM examinations reveal that these grains are made up of strongly agglomerated polyhedral crystallites, with little internal porosity [Fig. 4(a)]. For both oxides, the crystallite size ranges between 30 and 250 nm. A non-specific orientation of the crystallites gives rise to rings on the EMD pattern [Fig. 4(b)]. This microstructure is similar to that observed for $Mg_{0.9}Co_{0.1}Al_2O_4$ and $Mg_{0.9}Ni_{0.1}Al_2O_4$ solid solutions.[13]

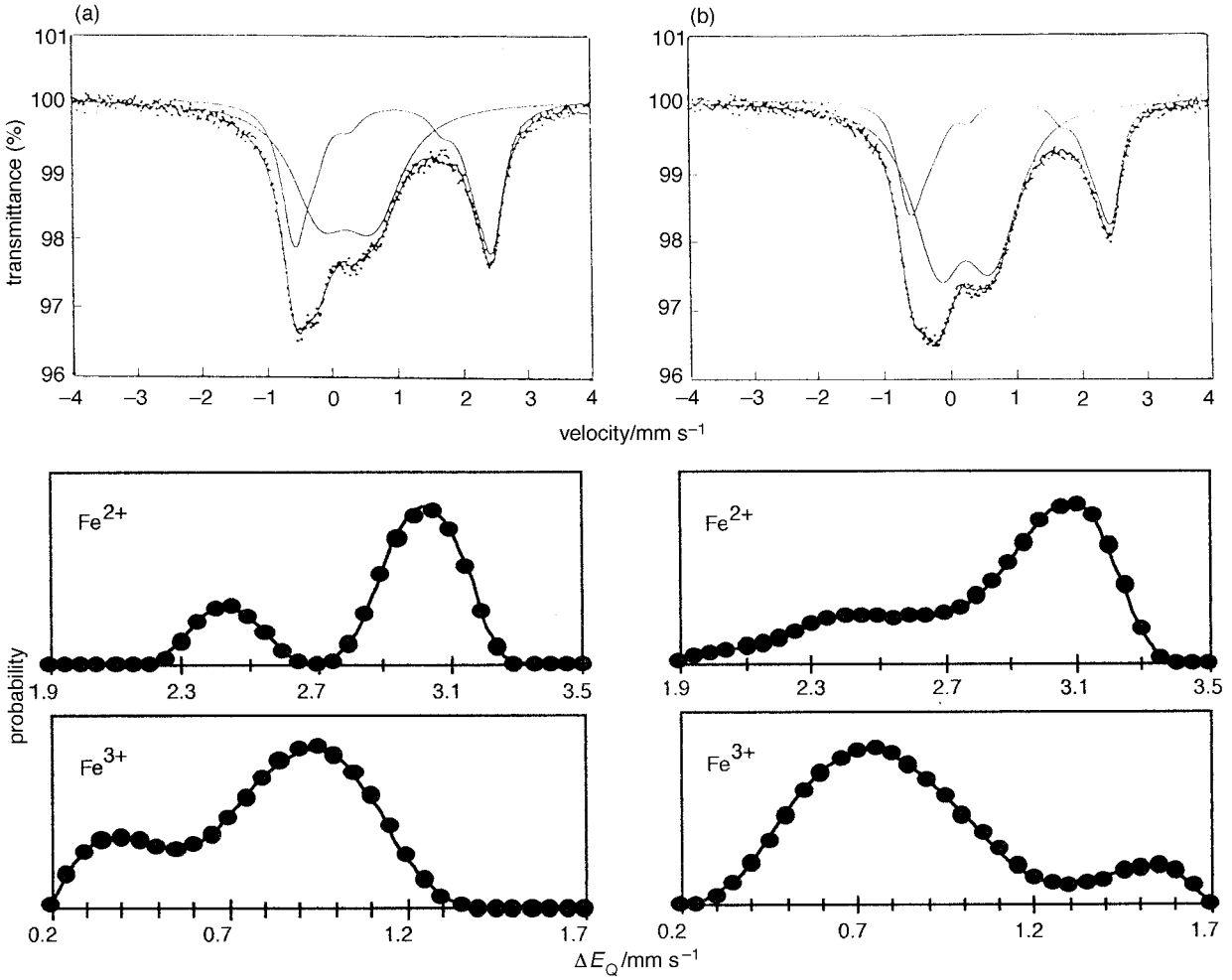

Fig. 2 Mössbauer spectra (9 K) of the as-prepared (a) Co- and (b) Ni-containing oxides and the corresponding quadrupole-splitting distributions for the Fe^{2+} and Fe^{3+} components

Table 2 Mössbauer parameters measured at 9 K of the as-prepared oxides[a]

		Fe^{2+}				Fe^{3+}			
specimen		δ	ΔE_Q	Γ	P	δ	ΔE_Q	Γ	P
Co-containing	(1)	1.07	2.45	0.42	45	0.37	0.40	0.95	55
oxide	(2)	1.05	3.05			0.35	0.95		
Ni-containing	(1)	1.08	2.45	0.31	33	0.35	0.75	0.78	67
oxide	(2)	1.05	3.10			0.41	1.55		

[a] δ = centre shift/mm s^{-1}; ΔE_Q: quadrupole splitting/mm s^{-1}; Γ = half width at half height/mm s^{-1}; P = proportion (%). The δ and ΔE_Q values are those of the two peaks detected in the quadrupole-splitting distribution profiles: notations (1) and (2) refer to the lower and higher quadrupole-splitting components, respectively.

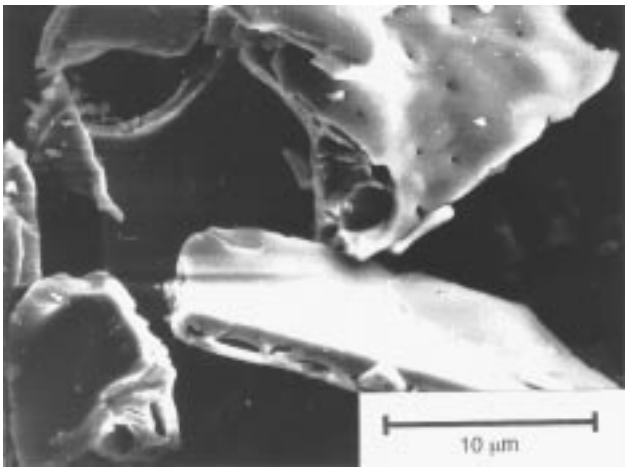

Fig. 3 SEM micrograph of the as-prepared Co-containing oxide

Nanocomposite powders

The as-prepared oxide powders have been reduced in hydrogen at T_r = 700, 750, 800, 850, 900, 950 and 1000 °C. For the sake of brevity, the resulting composite powders will be denoted as FeCoR700, FeCoR750, …, FeNiR1000 in the following section.

Analysis of the XRD patterns of the composite powders (Fig. 5) reveals the presence of a spinel as the major phase. Since the bcc Fe/Co (110) peak can not be resolved because of its superposition with the (400) spinel peak (measured interplanar distance 0.202 nm), we have calculated the ratio

$$R_1 = \frac{I_{400}(\text{spinel}) + I_{110}(\text{Fe/Co})}{I_{311}(\text{spinel})}$$

in which I_{400} and I_{311} represent the relative intensities of the spinel (400) and (311) peaks respectively and I_{110} that of the unresolved bcc Fe/Co (110) peak. R_1 is found to increase with increasing T_r up to 900 °C and then remains constant [Fig. 6(a)], which demonstrates the evolving formation of bcc Fe/Co alloy(s) and suggests that the reduction of the transition-metal ions is completed at 900 °C. The γ-Fe/Ni (111) and (200) peaks (measured inter-reticular distances 0.207 and 0.180 nm respectively) are clearly detected in the XRD patterns [Fig. 5(b)]. Their intensities increase with increasing T_r. Using

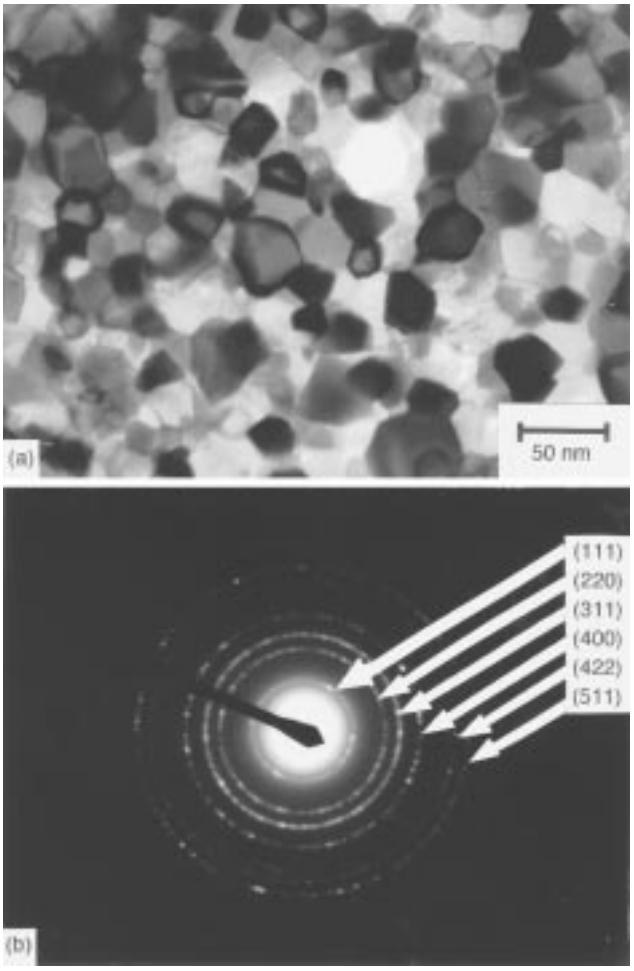

Fig. 4 TEM micrograph (a) and EMD pattern (b) of the as-prepared Co-containing oxide

the evolution of the ratio

$$R_2 = \frac{I_{111}(\mathrm{Fe/Ni})}{I_{311}(\mathrm{spinel})}$$

with I_{311} and I_{111} the relative intensities of the spinel (311) and the Fe/Ni (111) peaks respectively, one can approximately follow the reduction of the oxide with the increase in T_r [Fig. 6(b)]. R_2 keeps increasing in the entire temperature range (700–1000 °C), indicating that the reduction of the transition metal ions is not complete below 1000 °C. These findings are in good agreement with an earlier work[13] showing that the reduction of the transition metal ions to the metallic state in $Mg_{0.9}Co_{0.1}Al_2O_4$ and $Mg_{0.9}Ni_{0.1}Al_2O_4$ solid solutions was complete at 900 and 1000 °C, respectively.

The specific surface areas of the Fe/M-$MgAl_2O_4$ powders decrease with increasing T_r (Fig. 7). The values measured for the FeCoR1000 and FeNiR1000 composites (1.1 and 1.6 $m^2\ g^{-1}$ respectively) are close to those reported for the Co- and Ni-$MgAl_2O_4$ composites obtained by reduction at 1000 °C (1 $m^2\ g^{-1}$).[13] SEM observations reveal no change in the morphology and microstructure as compared to the oxide. TEM observations have been performed on the composite powders and reveal metal nanoparticles homogeneously dispersed in the oxide matrix (Fig. 8). The metal particles are pictured as small, dark areas on the micrographs as can be seen by comparing the images of the oxide [Fig. 4(a)] and of the composites [Fig. 8(b) and (c)]. The number of particles is higher in the R900 and R1000 composites than in R700 and R800 specimens. It is interesting to note the presence of a shell, about 2 nm thick, surrounding the metal particles in the FeCoR800 composite [Fig. 8(a)]. Such a core–shell nanostructure has been observed earlier in Fe/Ru-Al_2O_3 and Fe-Al_2O_3 nanocomposite powders: in the former case,[7] it points to a bimetallic nature of the nanoparticles (Ru-rich core and Fe-rich shell) and in the latter case[11] at Fe particles (core) separated from the Al_2O_3 matrix by a thin $FeAl_2O_4$ layer (shell) which is formed because the reduction temperature was sufficiently low (800 °C) in order not to totally reduce the Fe ionic species to metallic iron. The explanation given for the Fe/Ru-Al_2O_3 nanocomposite can probably be ruled out in the present case since Fe and Co cannot be distinguished from one another at the TEM magnification used in this study (×100 000). High-resolution electron microscopy would be helpful to clarify this point.

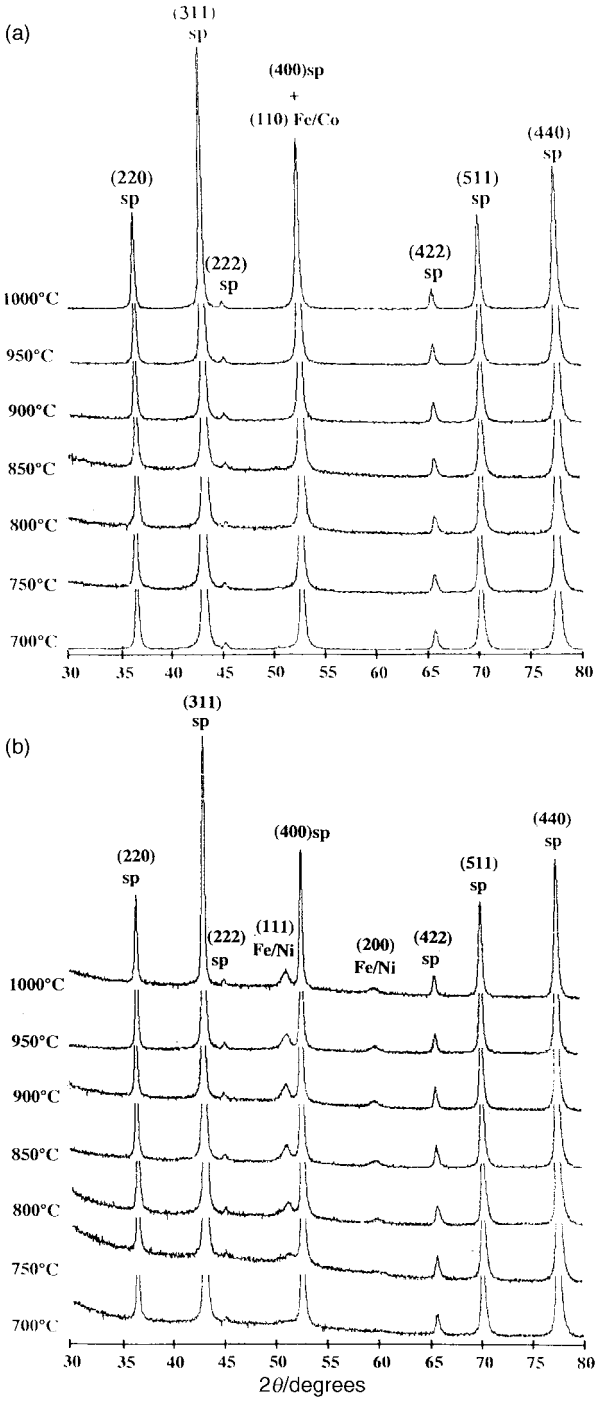

Fig. 5 XRD patterns of the Fe/Co-$MgAl_2O_4$ (a) and Fe/Ni-$MgAl_2O_4$ (b) powders prepared by reduction at different temperatures (sp, spinel phase)

The metal-particles size distributions (in number) were derived from the measurement of the size of about 200 particles

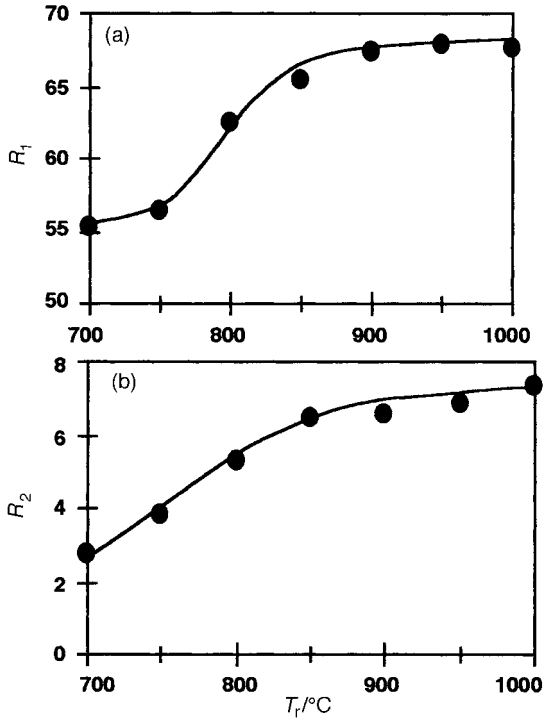

Fig. 6 Evolution of R_1 (a) and R_2 (b) with the reduction temperature (T_r). See text for the definitions of R_1 and R_2.

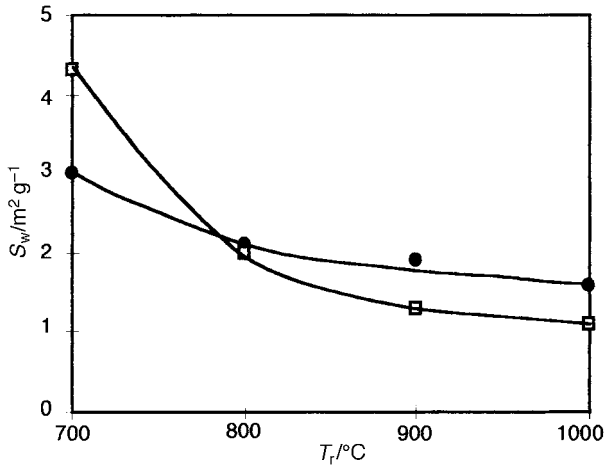

Fig. 7 Evolution of the specific surface area (S_w) of Fe/Co-$MgAl_2O_4$ (●) and Fe/Ni-$MgAl_2O_4$ (□) composite powders with the reduction temperature (T_r)

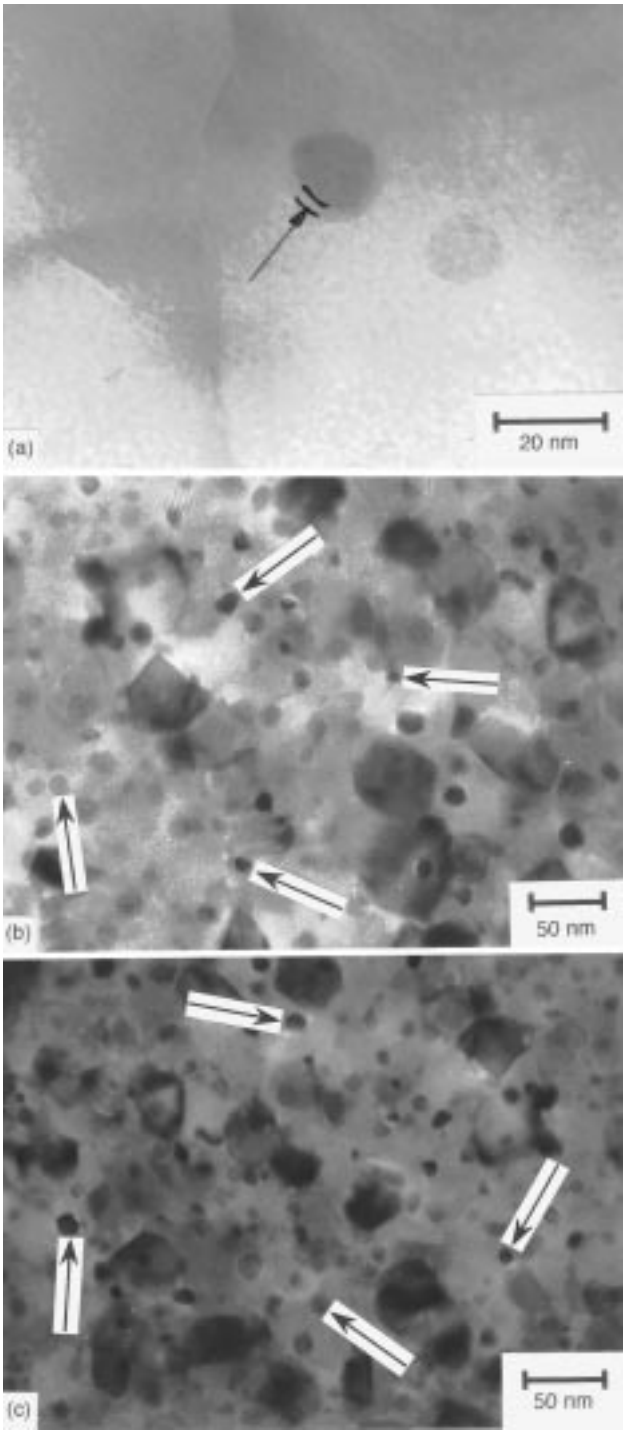

Fig. 8 TEM micrographs of the Fe/Co-$MgAl_2O_4$ powder prepared by reduction at 800 °C (a) and 1000 °C (b) and of the Fe/Ni-$MgAl_2O_4$ powder prepared by reduction at 1000 °C (c). In (a), the arrow indicates an oxide shell at the surface of a Fe/Co particle. In (b) and (c), some metal particles, appearing as small dark dots, are pointed out by the arrows; some larger dark areas are probably matrix grains in or near the Bragg position with respect to the electron beam. Comparison with a TEM image of the metal-free $MgAl_2O_4$ powder [Fig. 4(a)] may help the reader to distinguish between the different phases.

pictured on the original TEM negatives (Fig. 9). In all cases, the size distributions are unimodal and rather narrow. Previous works[5,8] have shown that this feature mainly results from the monophase nature of the starting oxide solid solutions and also from their relatively low specific surface area. The average size of the metal particles increases with increasing T_r, from 6.3 to 12.5 nm for FeCoR700 and FeCoR1000 respectively, and from 6.5 to 10.1 nm for FeNiR700 and FeNiR1000 respectively. The position of the peak in the distribution follows a similar evolution. The rather high average size (11.4 nm) obtained for the FeCoR800 specimen is due to the presence of the above discussed shell around the particles. One can also observe that the increase in T_r from 900 to 1000 °C gives rise to a marked broadening of the Fe/Co particle-size distribution. This could indicate that the reduction of the transition metal ions is completed at 900 °C, in line with the XRD observations, and that a higher reduction temperature only results in a coalescence of the metal particles. In contrast, such a phenomenon is not observed in the case of the Fe/Ni-$MgAl_2O_4$ composites.

The metal nanoparticles were further examined by EDX analysis. In contrast to previous results on Fe/Cr-Al_2O_3 powders,[6] no correlation has been found between the composition and the size of the particles. However, the EDX results (Table 3) show that an increase in T_r leads to a more narrow composition range on the one hand and to an average composition closer to the desired one ($Fe_{0.65}M_{0.35}$, M = Co or Ni) on the other

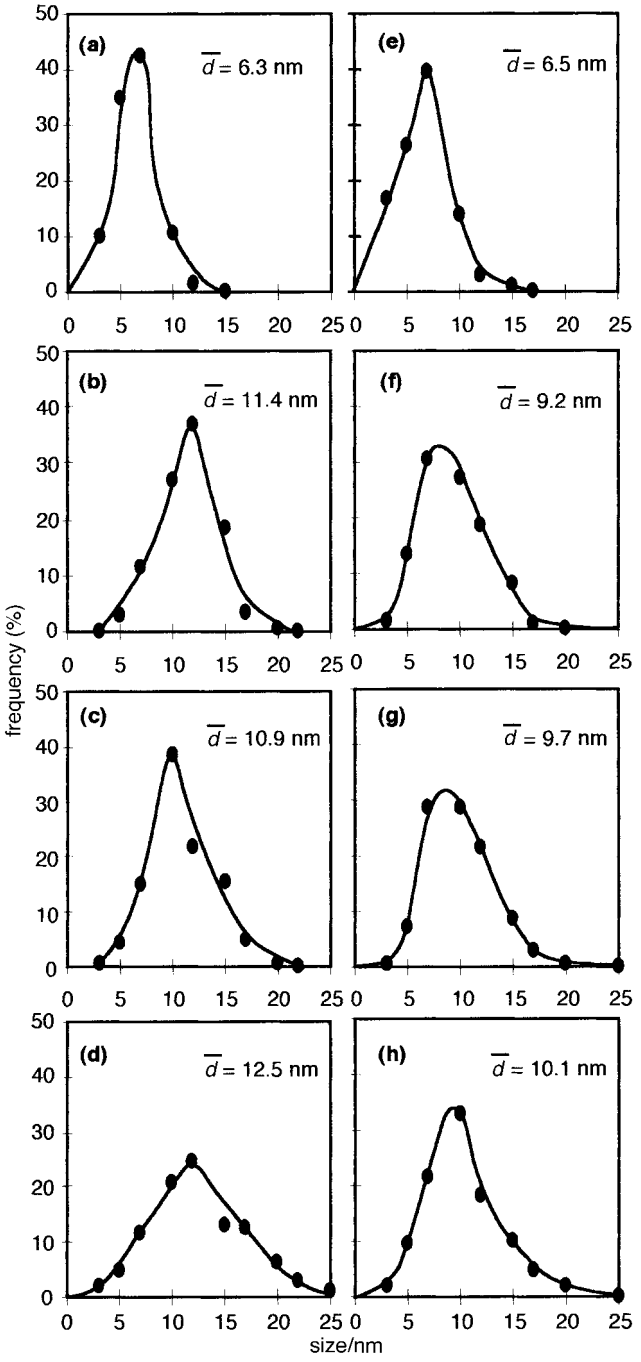

Fig. 9 Size distribution of the metal particles in the Fe/Co-$MgAl_2O_4$ composites prepared by reduction at (a) 700, (b) 800, (c) 900 and (d) 1000 °C, and in the Fe/Ni-$MgAl_2O_4$ composites prepared by reduction at (e) 700, (f) 800, (g) 900 and (h) 1000 °C

hand. The particles become more rich in Fe with increase in T_r, showing that the Co^{2+} and Ni^{2+} ions are more easily reducible than the Fe^{2+} ions. As the reduction proceeds, more Fe enters the previously formed Co (or Ni)-rich metallic lattice, eventually achieving the target composition, the difference with the observed one being within the precision limits of the EDX technique (±2 atom%). It is noteworthy that for a given specimen, the results for all analyzed particles fall within a certain composition range, in contrast to what has been observed in Fe/Ni-MgO powders,[10] in which the metal particles are distributed between at least two composition populations whatever the reduction conditions. The reason for this is, as yet, not clearly understood so far and will be the subject of future studies.

The Mössbauer spectra of the Fe/Co-$MgAl_2O_4$ and Fe/Ni-$MgAl_2O_4$ composites, obtained after reduction at 700, 800, 900 and 1000 °C, have been recorded at 9 K. They have been fitted with a doublet representing the Fe^{2+} ions and a sextet accounting for the ferromagnetic Fe/Co or Fe/Ni alloys. Fe^{3+} ions were not detected, meaning that the reduction to the iron(II) state is complete at temperatures below 700 °C. As mentioned earlier, this observation suggests that the Fe^{3+} ions are located at or near the surface of the oxide crystallites: indeed, the corresponding reduction temperature (≤700 °C) is considerably lower than those reported for Fe^{3+} ions substituting in the lattices of Al_2O_3 (1300 °C),[6] MgO (1200 °C)[10] and Cr_2O_3 (1200 °C).[22] The evolution of the Fe^{2+}/Fe^0 proportions, calculated from the relative spectral area of the doublet with respect to the sextet, allows one to quantify the reduction of the Fe^{2+} ions with the increase in T_r.

Table 3 Composition range and average composition of the metal nanoparticles in the Fe/Co-$MgAl_2O_4$ and Fe/Ni-$MgAl_2O_4$ composite powders. Δ (%) represents the difference between the maximum and minimum measured Co or Ni content in the metal particles of a given nanocomposite powder

specimen	composition range (±2 atom%)	Δ (%)	average composition (±2 atom%)
FeCoR700	$Fe_{0.47}Co_{0.53}$–$Fe_{0.62}Co_{0.38}$	0.09	$Fe_{0.47}Co_{0.53}$
FeCoR800	$Fe_{0.54}Co_{0.46}$–$Fe_{0.63}Co_{0.37}$	0.09	$Fe_{0.58}Co_{0.42}$
FeCoR900	$Fe_{0.60}Co_{0.40}$–$Fe_{0.65}Co_{0.35}$	0.05	$Fe_{0.62}Co_{0.38}$
FeCoR1000	$Fe_{0.61}Co_{0.39}$–$Fe_{0.66}Co_{0.34}$	0.05	$Fe_{0.63}Co_{0.37}$
FeNiR700	$Fe_{0.31}Ni_{0.69}$–$Fe_{0.67}Ni_{0.33}$	0.36	$Fe_{0.50}Ni_{0.50}$
FeNiR800	$Fe_{0.45}Ni_{0.55}$–$Fe_{0.70}Ni_{0.30}$	0.25	$Fe_{0.59}Ni_{0.41}$
FeNiR800	$Fe_{0.62}Ni_{0.38}$–$Fe_{0.68}Ni_{0.32}$	0.06	$Fe_{0.62}Ni_{0.38}$
FeNiR1000	$Fe_{0.60}Ni_{0.40}$–$Fe_{0.65}Ni_{0.35}$	0.05	$Fe_{0.64}Ni_{0.36}$

First, the Mössbauer spectrum of the Fe/Co-$MgAl_2O_4$ composites (Fig. 10 and Table 4) will be discussed. The proportion of Fe^{2+} ions sharply decreases from 84 to 9% on increasing T_r from 700 to 800 °C, eventually reaching 0% for $T_r \geq 900$ °C. This confirms that the reduction of this system is completed at 900 °C. The Fe/Co particles, the proportion of which accordingly increases, exhibit the same value for the hyperfine field ($H = 367$ kG) although their composition is different from one composite to the other as discussed above. This finding is in agreement with the room-temperature Mössbauer-spectroscopy study of Johnson *et al.*[23] which revealed a nearly constant H value ($H = 365$ kG) in the $Fe_{0.80}Co_{0.20}$–$Fe_{0.65}Co_{0.35}$ composition range.

For the Fe/Ni-$MgAl_2O_4$ composites (Fig. 11 and Table 5), the Mössbauer results confirm that the reduction is complete only at 1000 °C. It may thus be inferred that the reduction of Co^{2+} ions promotes the Fe^{2+} reduction more efficiently than the reduction of Ni^{2+} ions. Moreover, it should be noted that Fe/Ni-$MgAl_2O_4$ composites are much more easily prepared than Fe/Ni-MgO composites (total reduction at 1300 °C only).[10] It is further worth mentioning that no ferromagnetic α-Fe/Ni has been detected (neither by Mössbauer spectroscopy at 9 K, nor in the XRD patterns), showing that the martensitic $\gamma \rightarrow \alpha$ transformation upon cooling is suppressed in fine alloy particles containing >20 atom% Ni, as indicated on the Fe–Ni phase diagram proposed by Hansen.[24] Since the $\gamma \rightarrow \alpha$ transformation temperature dramatically increases with decreasing Ni content,[24] this also confirms the present EDX results detecting no alloy particles with <35 atom% Ni.

The hyperfine field distribution $P(H)$ of the sextets (Fig. 11) is broad, ranging between 250 and 400 kG. It has not been necessary to consider lower hyperfine field values to obtain acceptable fits, in contrast to what has been claimed by Gonser *et al.*,[25] who reported a field distribution with two broad maxima centred around 80 and 300 kG at 22 K under an external field of 5 T. These authors assigned the high-field component to a ferromagnetic ordering of the alloy and the

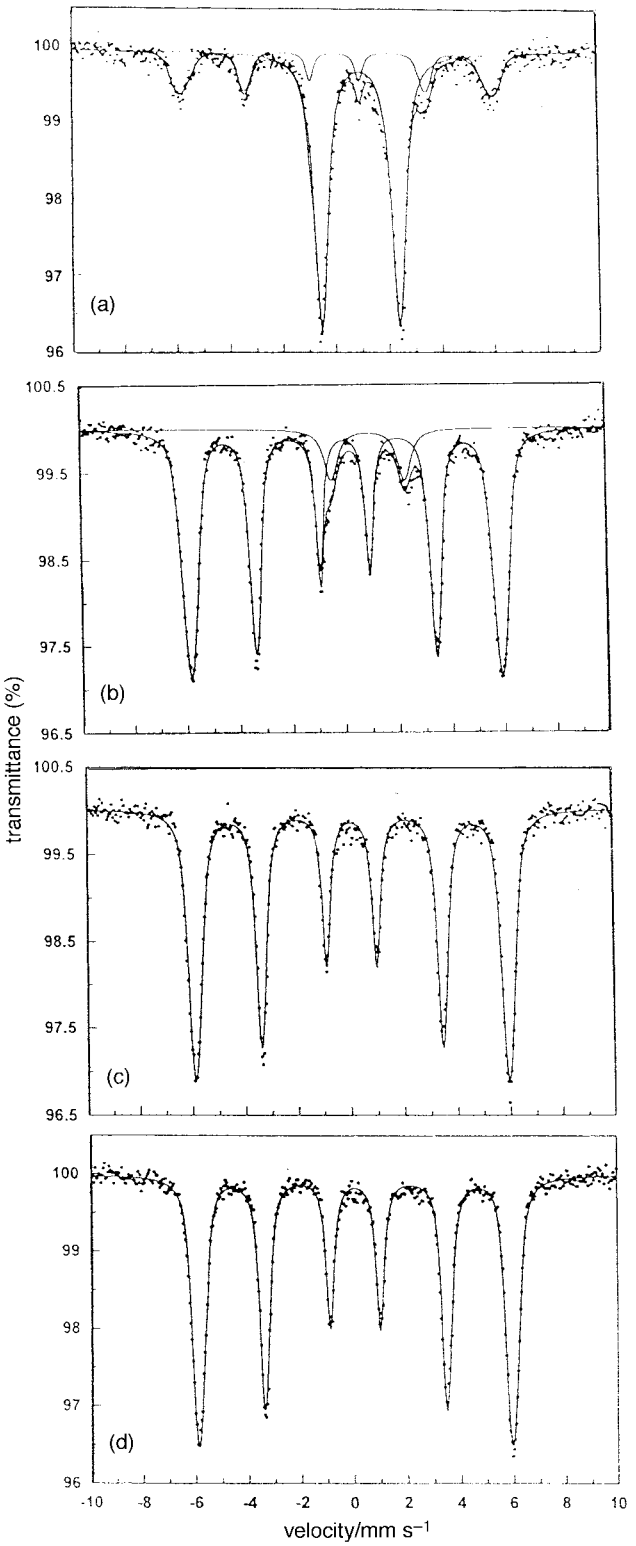

Fig. 10 Mössbauer spectra (9 K) of the Fe/Co-$MgAl_2O_4$ powders prepared by reduction at (a) 700, (b) 800, (c) 900 and (d) 1000 °C

low-field one to an antiferromagnetic ordering at low temperature. Our hyperfine field distributions show several peaks, the number and positions of which depend upon T_r. Similar line shapes have been reported by several different authors for ferromagnetic γ-$Fe_{1-x}Ni_x$ alloys.[25–29] Since the Ni content in Fe/Ni alloys is known to have a strong influence on the hyperfine field of the corresponding sextets,[23] the observed field distribution line shapes in the present Fe/Ni alloys could reflect the compositional fluctuations suggested by the EDX results. In the case of FeNiR700, one can assume that the contribution of the sextet to the total MS is too low [Fig. 11(a)] to derive information from the corresponding $P(H)$ pattern. For the other specimens, it seems that the field distribution between 300 and 400 kG becomes more narrow with increasing T_r. Indeed, the two peaks which are clearly resolved for the FeNiR800 composite are less easily distinguished in the pattern of FeNiR900 and only a large, single peak (with a shoulder on the high-field side) is observed for FeNiR1000. This may reflect the higher compositional homogeneities (from particle to particle) with increasing T_r, as observed by EDX analysis. A small peak (centred around 290 kG) is present in the four $P(H)$ patterns. Its origin has remained unclear.

The Mössbauer spectrum of the FeCoR1000 and FeNiR1000 composites have also been recorded at 298 K. The Mössbauer spectrum of FeCoR1000 (Fig. 12 and Table 6) consists of only a sextet, representing ferromagnetic bcc Fe/Co alloy(s). The hyperfine field of this sextet (365 kG) is in good agreement with the results of Johnson *et al.*[23] The Mössbauer spectrum of the FeNiR1000 powder [Fig. 13(a) and Table 6] shows a sextet accounting for ferromagnetic Fe/Ni alloy(s) and a singlet, the area of which represents 20% of the total spectrum. The value of the average hyperfine field $\bar{H}$ of the sextet (300 kG) confirms that the composition of the particles obtained after reduction at 1000 °C is close to the desired one ($Fe_{0.65}Ni_{0.35}$).[23,25,30] The field distribution is broad [Fig. 13(b)], ranging between 200 and 340 kG, with a peak at about 300 kG and a strong shoulder on the low-H side (about 240 kG). It is probable that the shoulder and peak correspond to those observed on the 9 K data plot at *ca.* 290 and 340 kG.

Interestingly, the appearance of the singlet reflects the presence of a phase which is non-ferromagnetic at 298 K. Similar spectra have first been reported on γ-Fe/Ni alloys with 30, 32 and 34 atom% of Ni, from room temperature down to liquid-N_2 temperature, by Nakamura *et al.*[31] These authors concluded that the singlet may originate from antiferromagnetic regions, the Néel temperature of which may be well below liquid-N_2 temperature. This explanation was reported to be in agreement with the antiferromagnetic coupling of iron moments as proposed by Kondorsky and Sedov[16] to account for the decrease of the bulk magnetic moments in the Invar alloys. There has been considerable debate concerning the origin of these antiferromagnetic regions in γ-Fe/Ni Invar alloys and several models have been proposed to explain this feature. Weiss[30] considered that the Fe atoms in the fcc lattice can exist in two different electronic structures closely spaced in energy (γ_1 and γ_2, corresponding to antiferro- and ferromagnetic coupling, respectively) and that alloying with a metal such as Ni, Pd or Pt can stabilize the γ_2 level. Thermal excitation of the γ_1 level would then lead to a marked decrease in the Curie temperature because of the reversed sign of the exchange interaction in this γ_1 state. Kachi and Asano[32] proposed that fluctuations of the local Ni concentration around a critical value in the 30–35 atom% range would result in Ni-rich parts forming ferromagnetic clusters owing to the strong Fe–Ni and Ni–Ni ferromagnetic couplings, and in Fe-rich regions forming clusters within which antiferromagnetic coupling is predominant. Several authors[27,33,34] found that a good description of their experimental results was obtained with minor modifications of this latter model. In particular, Menshikov *et al.*[33] claimed to have observed such a phenomenon for a bulk $Fe_{0.65}Ni_{0.35}$ alloy and estimated the size of the non-ferromagnetic regions to be about 1 nm. Ullrich and Hesse[28] studied bulk γ-Fe/Ni Invar alloys in the concentration range of 30–36 atom% of Ni and proposed, in opposition to Weiss 'electronic model',[30] a so-called 'magnetic model' that assumes the existence of a non-parallel arrangement of Fe moments. All their Mössbauer spectra could be interpreted by this model regardless of the Ni content (30–36 atom%) and the temperature. Rancourt *et al.*[35] also observed the coexistence of both paramagnetic and ferromagnetic contributions to the room-temperature Mössbauer spec-

Table 4 Mössbauer parameters (9 K) of the Fe/Co-$MgAl_2O_4$ composites prepared by reduction at different temperatures[a]

	Fe^{2+}				ferro-Fe/Co				
composite	δ	ΔE_Q	Γ	P	H	δ	$2\varepsilon_Q$	Γ	P
FeCoR700	1.05	2.86	0.55	84	367	0.12	0.00	0.30	16
FeCoR800	1.04	2.78	0.57	9	366	0.14	0.00	0.34	91
FeCoR900	—	—	—	—	366	0.15	0.00	0.36	100
FeCoR1000	—	—	—	—	367	0.15	0.00	0.36	100

[a] H = hyperfine field/kG; δ = centre shift/mm s^{-1}; ε_Q and ΔE_Q = quadrupole splitting/mm s^{-1}; Γ = half width at half height/mm s^{-1}; P = proportion (%); ferro = ferromagnetic.

trum of a synthetic bulk $Fe_{0.65}Ni_{0.35}$ alloy. They proposed that these contributions respectively arise from metastable precipitates of a low-spin γ-Fe/Ni phase (γ_{LS}) embedded in a matrix of high-spin γ-Fe/Ni phase (γ_{HS}, the ordinary quenched Fe/Ni phase) of the same controlled composition. They point out that this model is not to be confused with that of Weiss because γ_{LS} could occur as a distinct phase. It is also worth mentioning that this model was successfully applied to specimens of the Santa Catharina meteorite,[36,37] a material that contains several Fe/Ni phases. However, detailed low-temperature, in-field Mössbauer spectroscopy studies on several slices of the same meteorite[38] have led to the conclusion that the unsplit line probably arises from a $Fe_{0.72}Ni_{0.28}$ phase, the magnetic nature of which may be described as a mixture of paramagnetic and ferromagnetic parts owing to slight composition fluctuations. The singlet observed in the present Mössbauer spectrum of the nanocomposite powders could *a priori* account for either a superparamagnetic, a paramagnetic or an antiferromagnetic phase. Indeed, superparamagnetic behaviour has been reported for Fe/Ni alloys in the forms of thin foils[39] and fine particles.[40] A paramagnetic γ-phase has been detected by Widatallah *et al.*[41] on fcc $Fe_{0.90}Ni_{0.10}$ fine particles, a composition which is quite far from that of the present particles. Baldokhin *et al.*[42] observed coexistence of paramagnetism and ferromagnetism on $Fe_{0.65}Ni_{0.35}$ fine particles (between 5 and 15 nm in diameter) and proposed explanations according to Weiss's model.[30]

In order to get more information on the origin of the room-temperature single line and to determine the magnetic nature of the corresponding phase, which seems to be ferromagnetic at 9 K, a spectrum of the FeNiR1000 powder was measured at 275 K in a 6 T external field applied parallel to the γ-ray beam. The resulting Mössbauer spectrum consists of two subspectra [Fig. 13(c)], showing that the phase giving rise to the singlet in the zero-field Mössbauer spectrum is not superparamagnetic. A fit has been attempted assuming that one subspectrum was the quadruplet of the ferromagnetic phase, the second one being a sextet (fixed area ratio 3:2:1) representing an antiferromagnetic alloy. The result was a poor description of the central part of the spectrum. The best fit has been obtained assuming that two quadruplets (fixed area ratio 3:0:1) composed the total spectrum. The first quadruplet (δ = 0.01 mm s^{-1}, $2\varepsilon_Q \approx 0$ mm s^{-1}, $\bar{H}$ = 258 kG) represents the ferromagnetic γ-Fe/Ni phase. The second one ($\delta = -0.02$ mm s^{-1}, $2\varepsilon_Q \approx 0$ mm s^{-1}, $\bar{H}$ = 45 kG) is consistent with a paramagnetic γ-Fe/Ni phase and its proportion (20%) corresponds to that of the singlet in the spectrum recorded without applied field.

One can consider several mechanisms to explain the paramagnetic behaviour observed for the FeNiR1000 composite. Existence of two states of the iron atoms as proposed by different authors[30,35] can be ruled out because the Mössbauer spectrum of FeNiR1000 recorded at 9 K shows only one sextet representative of a ferromagnetic alloy. According to Kachi and Asano,[32] paramagnetism could also appear due to fluctuations of the Ni content. In the present case, one has to consider the fluctuations that most probably exist from one alloy particle to the other (as indicated by the EDX results) on the one hand and concentration inhomogeneities within a given alloy particle on the other hand. In the latter case, one may assume that the surface alloy particles, which are formed first, are more homogeneous than the intragranular ones, for which the slight differences in Ni^{2+} and Fe^{2+} ions reduction temperatures could have provoked a composition gradient. Thus, the intragranular particles would have a Ni-rich internal part and a Fe-rich external part, leading to the ferromagnetic and paramagnetic behaviours respectively. The observed proportion of paramagnetic phase (20%) would correspond to an Fe-rich zone extending over the two external atomic layers of a metallic particle 10 nm in diameter (and thus containing about 25 atomic layers). Such an explanation is not unrealistic. Another possibility is that the room-temperature paramagnetic behaviour is due to some very small Fe/Ni particles, the Curie temperature of which is known to strongly decrease with decreasing particle size.[24] The data obtained so far do not allow one to discriminate between these assumptions, but other results, presented hereafter, seem to point out that interparticular concentration fluctuations are most likely involved in the observed room-temperature paramagnetism.

Oxidation of the nanocomposite powders

The oxidation behaviour of the FeCoR1000 and FeNiR1000 powders was investigated by heating them in air up to 1100 °C in a thermobalance. XRD analysis showed that the oxidation products consist of spinel phases similar to the as-prepared oxides. Fe-, Co- or Ni-based oxides were not detected. The mass gain measured after the oxidation run (*ca.* 1.50%) corresponds to that of fully reduced 4 mass% $Fe_{0.65}Co_{0.35}$- and $Fe_{0.65}Ni_{0.35}$-$MgAl_2O_4$ nanocomposites. The differential thermogravimetry (DTG) curves (Fig. 14) show that the oxidation of the composites occurs in several steps, some of them at temperatures lower than 600 °C and others at temperatures exceeding 750 °C. From the conclusions of previous works on the oxidation of Fe/Cr-Al_2O_3 and Fe/Cr-Cr_2O_3[8] as well as Co- and Ni-$MgAl_2O_4$ nanocomposites,[13] it is inferred that the former steps corresponds to the oxidation of the metal particles located at the surface and in the open porosity of the oxide matrix and the latter ones to that of the intragranular metal particles. This has been evidenced by the DTG curves of powders which had been treated in HCl (boiling, 1 mol l^{-1}) prior to the thermal analysis, showing the low-temperature oxidation phenomena to be absent as the corresponding metal particles have been dissolved by the acid. On the contrary, the high-temperature oxidation phenomena remain unchanged because the oxide grains, which were not affected by the acid treatment, protected the metal particles dispersed within their matrix. It thus can roughly be estimated that more than two-thirds of the metallic phase (*ca.* 68% and 87% for FeCoR1000 and FeNiR1000, respectively) is dispersed as intragranular particles. A major difference with the oxidation behaviour of the Co- and Ni-$MgAl_2O_4$ nanocomposites[13] is the position of the high-temperature oxidation peak, which is about 160 °C lower in the present powders (780 and 800 °C in the Fe/Co- and Fe/Ni-$MgAl_2O_4$ composites respectively and 940 and 970 °C in the Co- and Ni-$MgAl_2O_4$ composites respectively).

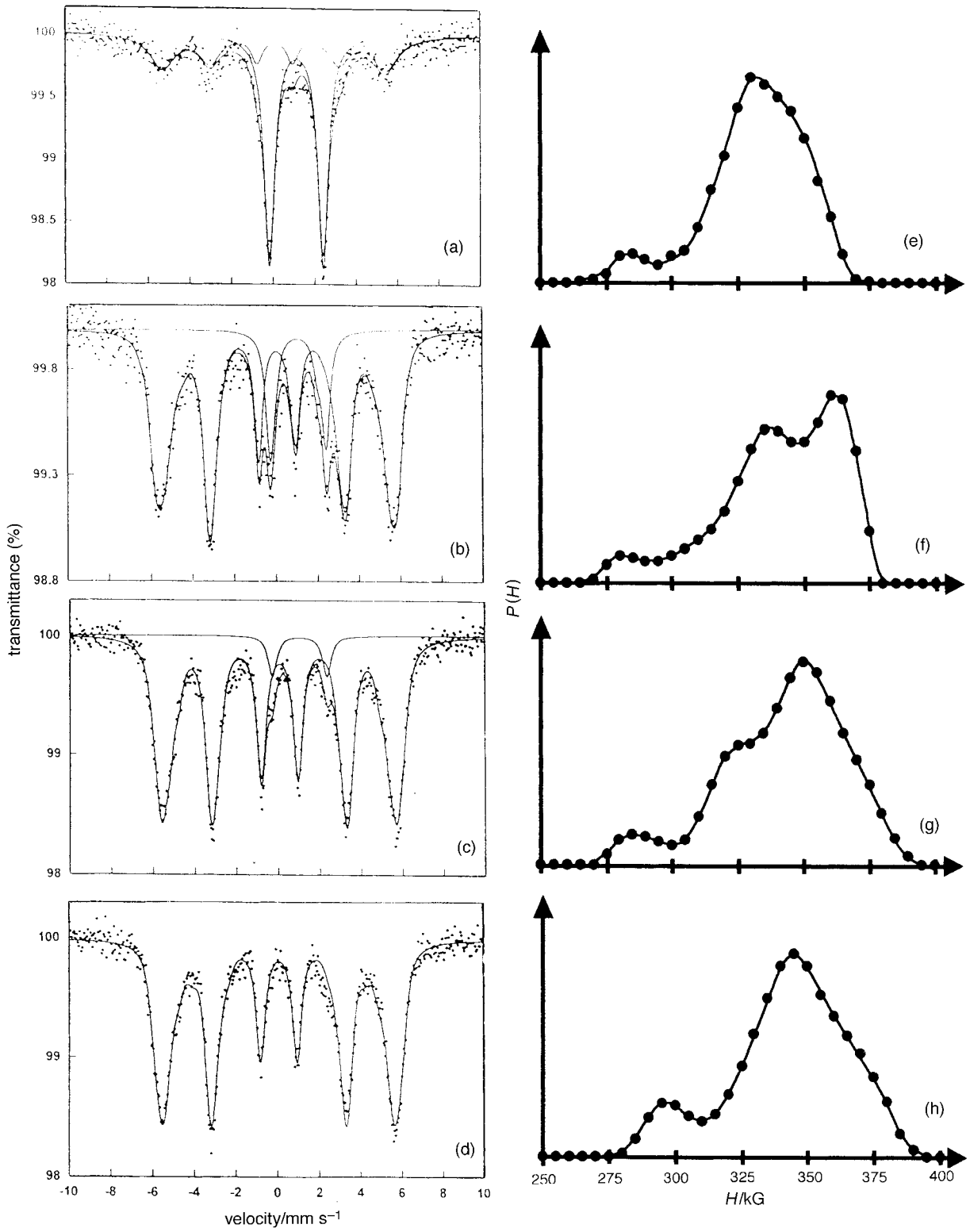

Fig. 11 Mössbauer spectra (9 K) of the Fe/Ni-$MgAl_2O_4$ powders prepared by reduction at (a) 700, (b) 800, (c) 900, (d) 1000 °C and the corresponding calculated field probability distributions (e, f, g, h respectively)

This obviously is related to the presence of iron, the Fe/Co and Fe/Ni alloy particles appearing to be more sensitive to air oxidation than pure Co and Ni particles.

The Mössbauer spectrum of the HCl-treated FeNiR1000 powder was recorded at room temperature. Assuming that all the surface Fe/Ni particles have been removed by the acid etching, we may consider that this spectrum is representative for the intragranular Fe/Ni alloy particles only. The best fit has been obtained assuming that the Mössbauer spectrum is composed of a sextet and a singlet. The sextet ($\delta =$ 0.03 mm s^{-1}, $2\varepsilon_Q \approx 0$ mm s^{-1}) has an average hyperfine field ($H = 300$ kG) characteristic of ferromagnetic $Fe_{0.65}Ni_{0.35}$ alloy.[23] The singlet ($\delta = 0.00$ mm s^{-1}) accounts for paramagnetic Fe/Ni. The proportions of the sextet and singlet are 89 and 11% of the total spectrum, respectively. Considering these figures and those derived from the Mössbauer spectrum of the untreated powder (ferromagnetic and paramagnetic Fe in the proportions 80:20) on the one hand and the fact that the intragranular Fe represents about 87% of the total Fe content on the other hand (we derive this latter figure from the TG

Table 5 Mössbauer parameters (9 K) of the Fe/Ni-$MgAl_2O_4$ composites prepared by reduction at different temperatures[a]

	Fe^{2+}				ferro-Fe/Ni				
composite	δ	ΔE_Q	Γ	P	$\bar{H}$	δ	$2\varepsilon_Q$	Γ	P
FeNiR700	1.22	2.62	0.61	60	333	0.17	0.01	0.96	40
FeNiR800	1.22	2.70	0.45	15	337	0.18	0.02	0.46	85
FeNiR900	1.15	2.61	0.41	5	350	0.18	0.01	0.41	95
FeNiR1000	—	—	—	—	346	0.18	0.00	0.47	100

[a] $\bar{H}$ = average hyperfine field/kG; δ = centre shift/mm s^{-1}; ε_Q and ΔE_Q = quadrupole splitting/mm s^{-1}; Γ = half width at half height/mm s^{-1}; P = proportion (%); ferro = ferromagnetic.

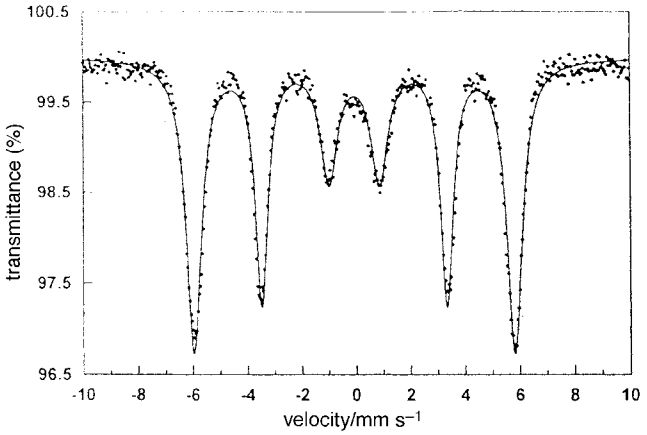

Fig. 12 Mössbauer spectrum (room temperature) of the Fe/Co-$MgAl_2O_4$ composite prepared by reduction at 1000 °C

Table 6 Mössbauer parameters measured at room temperature of the Fe/Co-$MgAl_2O_4$ and Fe/Ni-$MgAl_2O_4$ composites obtained after reduction at 1000 °C[a]

	ferro-Fe/M (M = Co or Ni)					non-ferro-Fe/Ni		
specimen	H	δ	$2\varepsilon_Q$	Γ	P	δ	Γ	P
FeCoR1000	365	0.04	0.00	0.65	100	—	—	—
FeNiR1000	300	0.04	0.03	0.57	80	0.00	0.78	20

[a] H = hyperfine field/kG; δ = isomer shift/mm s^{-1}; $2\varepsilon_Q$ = quadrupole shift/mm s^{-1}; Γ = half width at half height/mm s^{-1}; P = proportion (%); ferro = ferromagnetic.

measurements, assuming that there is no composition difference between the surface metal particles and the intragranular ones, so that the observed proportion of intragranular Fe/Ni alloy can be equated to the proportion of intragranular Fe), one may obtain a rough estimation of the proportions of the different Fe species with respect to the total metal content. Indeed, we find that the ferromagnetic and paramagnetic surface Fe account for 3 and 10%, respectively, whereas the ferromagnetic and paramagnetic intragranular Fe account for 77 and 10%, respectively. It appears that the paramagnetic particles are evenly distributed at the surface of the matrix grains and inside them. A striking feature is the very high proportion found for the ferromagnetic intragranular Fe. Since the intragranular particles are generaly smaller than the surface ones, it seems that these results rule out the above mentioned proposition that the room-temperature paramagnetism is based on a size effect, because one would then have observed a majority of paramagnetic intragranular metal particles. Furthermore, the large amount of ferromagnetic intragranular Fe is in opposition to the hypothesis of concentration fluctuations within individual particles being the main cause of room-temperature paramagnetism. Thus, we tentatively attribute this phenomenon to composition fluctuations from one alloy particle to the other. It is interesting to note that the critical composition below which our Fe/Ni alloy nanoparticles

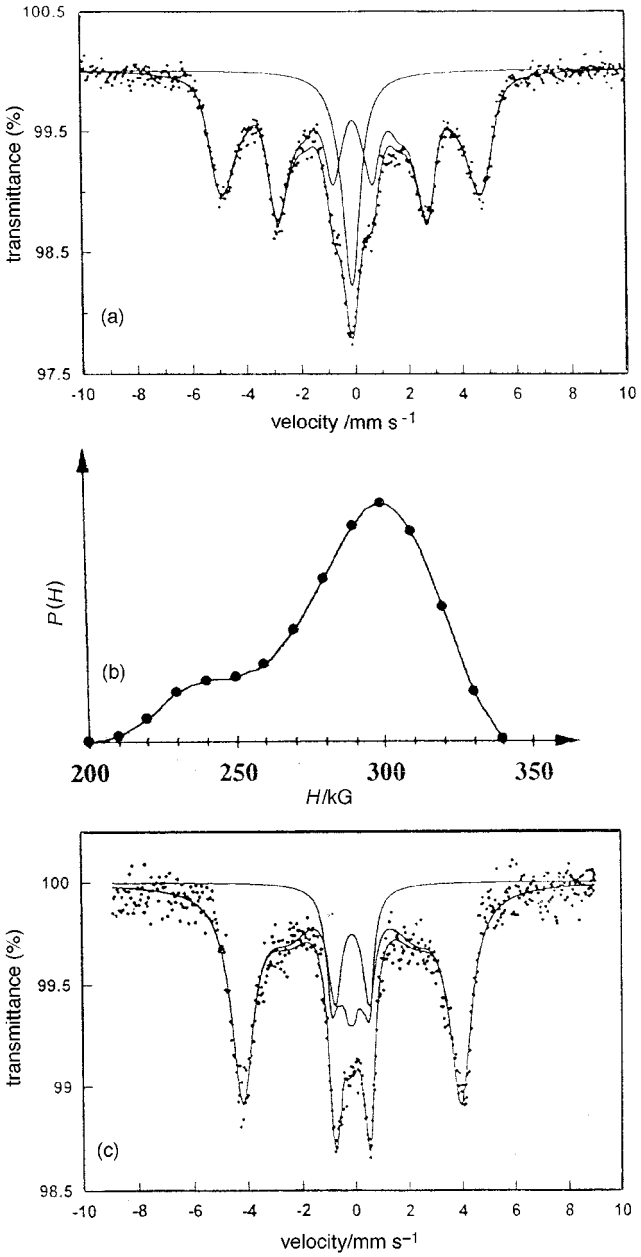

Fig. 13 Mössbauer spectrum (room temperature) of the Fe/Ni-$MgAl_2O_4$ composite prepared by reduction at 1000 °C (a), the calculated field probability distribution (b), and Mössbauer spectrum (room temperature) recorded under a 6 T external field (c)

are paramagnetic (between 35 and 40 Ni atom% in FeNiR1000) is of the order of, but slightly higher than the highest one (32 Ni atom%) reported by Kachi and Asano.[32] This difference in critical concentration could reflect a difference in size between the present alloy particles (*ca.* 10 nm) and those of Kachi and Asano[32] (*ca.* 10 μm).

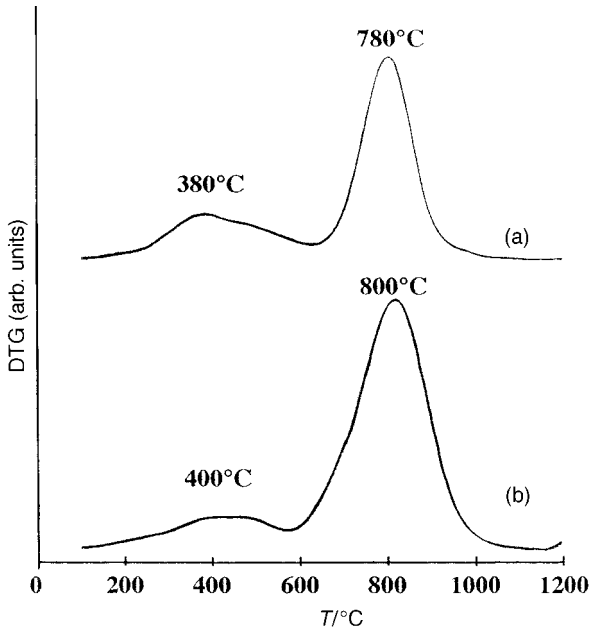

Fig. 14 DTG curves (measured in flowing air) of the Fe/Co-$MgAl_2O_4$ (a) and Fe/Ni-$MgAl_2O_4$ (b) powders prepared by reduction at 1000 °C

Conclusions

Fe/Co-$MgAl_2O_4$ and Fe/Ni-$MgAl_2O_4$ nanocomposite powders have been prepared by selective hydrogen reduction of oxide solid solutions of spinel structure synthesized by combustion in urea. Owing to the monophasic nature of the as-prepared oxides, the metallic alloy particles formed upon reduction are homogeneously dispersed in the spinel matrix. They are about 10 nm in diameter. The increase in reduction temperature from 700 to 1000 °C produces a narrowing of the particles composition range and an average composition closer and closer to the target one ($Fe_{0.65}Co_{0.35}$ and $Fe_{0.65}Ni_{0.35}$). It has been found that the Co^{2+} ions promote the reduction of the Fe^{2+} ions more efficiently than the Ni^{2+} ions; indeed, the reduction is completed at 900 and 1000 °C for the Fe/Co- and Fe/Ni-$MgAl_2O_4$ composites respectively. The Fe/Co and Fe/Ni particles are in the α (bcc) and γ (fcc) phases respectively. Mössbauer spectroscopy studies revealed that the Fe/Co particles are ferromagnetic at 9 K and room temperature. The Fe/Ni are ferromagnetic at 9 K but a significant fraction (20%) of Fe was found to be engaged in a paramagnetic phase at room temperature. This may be explained by composition fluctuations from one alloy particle to the other. Thermogravimetry indicates that the nanometric metal particles located at the surface and in the open porosity of the matrix are totally oxidized at temperatures lower than 600 °C, whereas those intragranularly dispersed are stable up to 800 °C. These latter particles account for more than two thirds of the total metal content.

This work has been sponsored in part by the Belgian 'Interuniversity Attraction Poles' program No. P4/10, Office of Scientific, Technical and Cultural Affairs. A 'Thematic Actions' grant of the Scientific Council of Université Paul-Sabatier, Toulouse, is also gratefully acknowledged.

References

1 D. Chakravorty, *Bull. Mater. Sci.*, 1992, **15**, 411.
2 S. Komarneni, *J. Mater. Chem.*, 1992, **2**, 1219.
3 R. Roy, *Mater. Res. Soc. Symp. Proc.*, 1993, **286**, 241.
4 Ch. Laurent and A. Rousset, *Key Eng. Mater.*, 1995, **108–110**, 405.
5 X. Devaux, Ch. Laurent and A. Rousset, *Nanostruct. Mater.*, 1993, **2**, 339.
6 Ch. Laurent, J. J. Demai, A. Rousset, K. R. Kannan and C. N. R. Rao, *J. Mater. Res.*, 1994, **9**, 229.
7 M. Verelst, K. R. Kannan, G. N. Subbanna, C. N. R. Rao, M. Brieu and A. Rousset, *Mater. Res. Bull.*, 1993, **28**, 293.
8 Ch. Laurent, Ch. Blaszczyk, M. Brieu and A. Rousset, *Nanostruct. Mater.*, 1995, **6**, 317.
9 V. Carles, M. Brieu, J. J. Demai and A. Rousset, in *Fourth Euro-Ceramics vol. 1*, ed. C. Galassi, Gruppo Editoriale Faenza Editrice S. p. A., 1995, p. 323.
10 V. Carles, M. Brieu and A. Rousset, *Nanostruct. Mater.*, in press.
11 X. Devaux, Ch. Laurent, M. Brieu and A. Rousset, *J. Alloys Compd.*, 1992, **188**, 179.
12 Ch. Laurent, A. Rousset, M. Verelst, K. R. Kannan, A. R. Raju and C. N. R. Rao, *J. Mater. Chem.*, 1993, **3**, 513.
13 O. Quénard, Ch. Laurent, M. Brieu and A. Rousset, *Nanostruct. Mater.*, 1996, **7**, 497.
14 C. E. Guillaume, *C. R. Acad. Sci. Paris*, 1897, **125,** 235.
15 R. M. Bozorth, in *Ferromagnetism*, D. Van Nostrand Company Inc., New York, 1951, p. 102.
16 E. I. Kondorski and V. L. Sedov, *J. Appl. Phys.*, 1960, **31**, 331S.
17 J. J. Kingsley and K. C. Patil, *Mater. Lett.*, 1988, **6**, 427.
18 K. C. Patil, *Bull. Mater. Sci.*, 1993, **16**, 6, 533.
19 S.R. Jain, K.C. Adiga and V.R. Pai Verneker, *Combust. Flame*, 1981, **40**, 71.
20 B. Hallstedt, *J. Am. Ceram. Soc.*, 1992, **75**, 1497.
21 A. Navrotsky and O. J. Kleppa, *J. Inorg. Nucl. Chem.*, 1967, **29**, 2701.
22 Ch. Laurent, Doctoral Thesis, Toulouse, 1994, 210 pp.
23 C. E. Johnson, M. S. Ridout and T. E. Cranshaw, *Proc. Phys. Soc.*, 1963, **81**, 1079.
24 M. Hansen, in *Constitution of Binary Alloys*, McGraw-Hill, New York, 1958, p. 678.
25 U. Gonser, S. Nasu and W. Kappes, *J. Magn. Magn. Mater.*, 1979, **10**, 244.
26 S. Tomiyoshi, H. Yamamoto and H. Watanabe, *J. Phys. Soc. Jpn.*, 1971, **30**, 1605.
27 H. Rechenberg, L. Billard, A. Chamberod and M. Natta, *Phys. Chem. Solids*, 1973, **34**, 1251.
28 H. Ullrich and J. Hesse, *J. Magn. Magn. Mater.*, 1984, **45**, 315.
29 I. Ortalli, A. Vera, G. Fratucello and F. Ronconi, *Hyperfine Interact.*, 1986, **28**, 1025.
30 R. J. Weiss, *Proc. Phys. Soc.*, 1963, **82**, 281.
31 Y. Nakamura, M. Shiga and N. Shikazono, *J. Phys. Soc. Jpn.*, 1964, **19**, 1177.
32 S. Kachi and H. Asano, *J. Phys. Soc. Jpn.*, 1969, **27**, 536.
33 A. Z. Menshikov, V. A. Shestakov and S. K. Sidorov, *Sov. Phys. JETP*, 1976, **43**, 86.
34 S. Komura and T. Tekada, *J. Magn. Magn. Mater.*, 1979, **10**, 191.
35 D. G. Rancourt, S. Chehab and G. Lamarche *J. Magn. Magn. Mater.*, 1989, **78**, 129.
36 R. B. Scorzelli, J. Danon and E. Galvao Da Silva, *Hyperfine Interact.*, 1986, **28**, 979.
37 D. G. Rancourt and R. B. Scorzelli, *J. Magn. Magn. Mater.*, 1995, **148**, 1.
38 E. De Grave, R. J. Pollard, R. E. Vandenberghe and P. M. A. de Bakker, *Hyperfine Interact.*, 1994, **94**, 2349.
39 J. Weissman and L. Levin, *Phys. Status Solidi A*, 1980, **60**, K201.
40 H. N. Ok and M. S. Han, *J. Appl. Phys.*, 1973, **44**, 1932.
41 M. Widatallah, R. S. Huang, Y. F. Hsia, X. M. Lee, J. H. Wang and H. X. Lu, *Hyperfine Interact.*, 1996, **1**, 278.
42 Yu. V. Baldokhin, P. Ya. Kolotyrkin, Yu. I. Petrov and E. A. Shafranovski, *J. Appl. Phys.*, 1994, **76**, 6496.

Paper 7/03773B; *Received* 30*th May*, 1997